ARTICLES
PUBLISHED ONLINE: 1 MAY 2017 | DOI: 10.1038/NPHOTON.2017.60
nature photonics

Dye-sensitized solar cells for efficient power generation under ambient lighting

Marina Freitag[1†], Joël Teuscher[2], Yasemin Saygili[1], Xiaoyu Zhang[3], Fabrizio Giordano[4], Paul Liska[4], Jianli Hua[3], Shaik M. Zakeeruddin[4], Jacques-E. Moser[2], Michael Grätzel[4]* and Anders Hagfeldt[1]*

Solar cells that operate efficiently under indoor lighting are of great practical interest as they can serve as electric power sources for portable electronics and devices for wireless sensor networks or the Internet of Things. Here, we demonstrate a dye-sensitized solar cell (DSC) that achieves very high power-conversion efficiencies (PCEs) under ambient light conditions. Our photosystem combines two judiciously designed sensitizers, coded D35 and XY1, with the copper complex Cu(II/I)(tmby) as a redox shuttle (tmby, 4,4′,6,6′-tetramethyl-2,2′-bipyridine), and features a high open-circuit photovoltage of 1.1 V. The DSC achieves an external quantum efficiency for photocurrent generation that exceeds 90% across the whole visible domain from 400 to 650 nm, and achieves power outputs of 15.6 and 88.5 μW cm^{-2} at 200 and 1,000 lux, respectively, under illumination from a model Osram 930 warm-white fluorescent light tube. This translates into a PCE of 28.9%.

Since the industrial revolution, humans have contributed more carbon dioxide to the atmosphere than Earth's plants can recycle, which has resulted in a global temperature rise. In 2016, CO_2 concentration in the atmosphere passed the mark of 400 ppm (refs 1,2) To realize a 'low–carbon society'[3], photovoltaics will play a key role in energy harvesting[4]. Next to the widely commercialized semiconductor technologies based on crystalline and thin-film Si solar cells, alternative photovoltaics are emerging[5]. Apart from thin-film systems such as $CuInGaSe_2$ (refs 6,7) or CdTe (ref. 6) cells, there has been a rapid development of perovskite solar cells[8–10] during the past five years. The latter evolved from dye-sensitized solar cells (DSCs), which themselves have recently undergone major advances as part of novel environmentally friendly photovoltaic technologies since their first report by Grätzel and co-workers[11,12].

Currently, the market for solar cells can be divided into large module installations for terrestrial power generation and smaller modules to power portable electronics[13]. DSCs can be used in both areas, but they hold particular promise within the second category. They show an outstanding performance under indoor, conditions with an artificial light source in comparison with other solar cell technologies[14]. The unique properties of DSCs make them the best alternative to wired and battery energy sources, as DSCs are capable of maintaining a high photovoltage even in diffuse light conditions[15–20].

DSCs are known to perform well in ambient light; however, very few studies have been published regarding the performance under such conditions. In addition, the few existing reports all use iodide-based electrolytes in combination with a ruthenium-based inorganic dye[21–23]. However, in 2005, Fukuzumi and co-workers reported that copper complexes worked well as redox mediators at reduced light intensities (~20 mW cm^{-2}) (ref. 24). The bis(2,9-dimethyl-1,10-phenanthroline) copper-based DSCs were further improved by Wang and co-workers by combining them with an organic sensitizer, which led to an increase in the power conversion efficiencies (PCEs) from 7.0% at 100 mW cm^{-2} to 8.3% at ~23 mW cm^{-2} air mass 1.5 global (AM 1.5G) light[25]. With further improvements of the DSCs and the introduction of new copper-based redox shuttles, Freitag and co-workers recently surpassed the 10.0% efficiency mark at 100 mW cm^{-2} AM 1.5G light for this family of alternative redox mediators[26–28].

Herein, for the first time, we introduce a DSC design that outperforms other photovoltaic technologies, including GaAs thin-film solar cells[29], in terms of efficiency and cost under ambient light conditions. By judiciously combining two previously reported chromophores[25], that is, the donor-π-acceptor (D-π-A) dye coded D35 (refs 30,31) and the recently discovered benzothiadiazole-based D-A-π-A sensitizer XY1 (ref. 32), we achieved highly effective light harvesting in the visible region extending from 400 to 650 nm and converted the absorbed photons to electrons with an external quantum efficiency (EQE) of 90% (ref. 33). Using these sensitizers in conjunction with the copper redox shuttle Cu(II/I)(tmby)$_2$ $TFSI_{2/1}$ (tmby, 4,4′,6,6′-tetramethyl-2,2′-bipyridine; TFSI, bistrifluoromethane sulfonimidate) we achieved a PCE of 28.9% under indoor conditions at 1,000 lux, where lux is the unit of light illuminance. Importantly, the cells maintain their high performance over a large domain of light intensities and spectral distributions, and yield a PCE of 11.3% in AM1.5G sunlight.

Results and discussion

Photovoltaic performance of co-sensitized DSCs with Cu(II/I)(tmby)$_2$ as redox shuttle. Here we exploit fully the advantages of the Cu(II/I)(tmby)$_2$ complexes, which are distinguished by a low reorganization energy that allows the regeneration of the sensitizer with a very small driving force of 0.1 V (ref. 25). The 'blend' of

[1]Laboratory of Photomolecular Science, Institute of Chemical Sciences and Engineering, École Polytechnique Fédérale de Lausanne (EPFL), 1015 Lausanne, Switzerland. [2]Photochemical Dynamics Group, École Polytechnique Fédérale de Lausanne (EPFL), 1015 Lausanne, Switzerland. [3]Key Laboratory for Advanced Materials and Institute of Fine Chemicals, School of Chemistry and Molecular Engineering, East China University of Science and Technology, 130 Meilong Road, Shanghai 200237, China. [4]Laboratory for Photonics and Interfaces, Institute of Chemical Sciences, Engineering École Polytechnique Fédérale de Lausanne (EPFL), 1015 Lausanne, Switzerland. †Present address: Department of Chemistry, Ångström Laboratory, Uppsala University, 75126 Uppsala, Sweden. *e-mail: michael.graetzel@epfl.ch; anders.hagfeldt@epfl.ch

© 2017 Macmillan Publishers Limited, part of Springer Nature. All rights reserved.

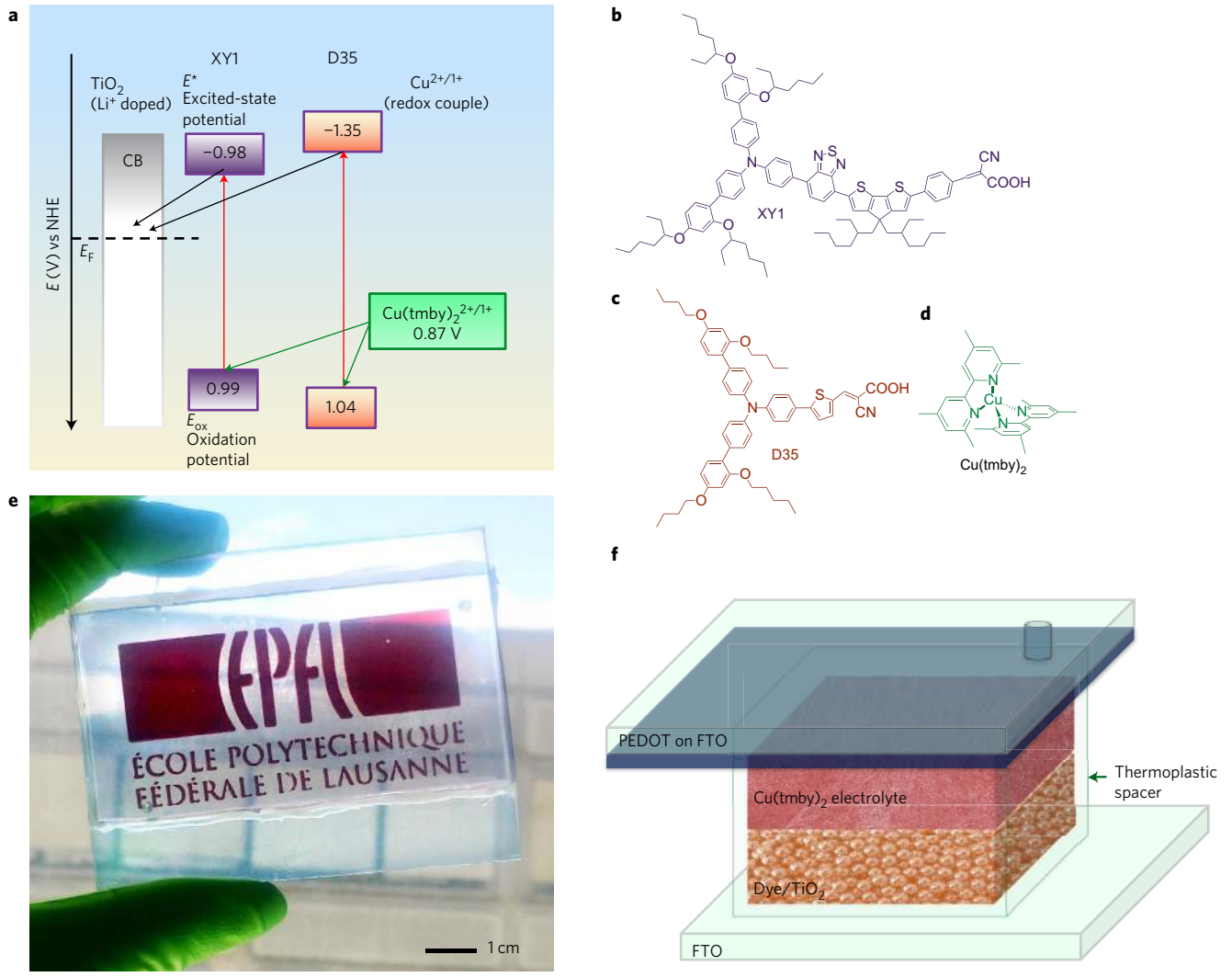

Figure 1 | Molecular photovoltaics with Cu(II/I)(tmby)$_2$ redox mediator and XY1 and D35 sensitizers. a, Schematic representation of the energy levels of the sensitizers XY1 and D35 with the Cu(tmby)$_2$ redox couple and possible electron-transfer processes. **b**–**d**, Molecular structures of the XY1 dye (**b**), D35 dye (**c**) and redox mediator Cu(tmby)$_2$ (**d**); the counterion is TFSI. **e**, Photograph of the DSC photoanode with the co-sensitized mesoporous TiO_2 films (EPFL logo) and PEDOT counter electrode. **f**, Schematic of a DSC.

organic chromophores (Fig. 1a) brings out the outstanding attributes of both dyes. The recently introduced XY1 sensitizer, a D-A-π-A dye, has a very high molar extinction coefficient and spectral response that extends beyond 700 nm, whereas D35 is an organic D-π-A dye endowed with a judiciously designed arylamine donor structure, which suppresses electron recapture by the Cu(II) complex from the TiO_2 conduction band and generates a high open-circuit potential[30,32]. Even during the early stage of this study we found that the XY1 dye in combination with D35 showed impressive photovoltaic metrics, specifically under indoor and ambient light illumination. A schematic representation of the energy levels in the device, and molecular structures of the D35 and XY1 dyes and the Cu(II/I) (tmby)$_2$ complexes are given in Fig. 1.

The solar cells were fabricated using a sandwich structure (Fig. 1e,f). The sensitized photoanode consisted of 8 µm of TiO_2 (4 µm 30NRD + 4 µm scattering layer) on a fluorine-doped tin oxide (FTO) substrate. Sensitization of the mesoporous TiO_2 layer was achieved by immersion into a dye solution with different dye ratios by varying the concentration of the sensitizers. The sensitizing solutions employed an equimolar mixture of acetonitrile and *tert*-butanol as solvent and contained the organic dyes in the molar ratios listed in Supplementary Table 1.

Using a thermoplastic spacer, we contacted the sensitized film with a poly(3,4-ethylenedioxythiophene) (PEDOT)-covered FTO conducting glass that served as the counter electrode[34]. The copper redox mediator that contained the electrolyte was introduced through a hole in the back electrode. The electrolyte employed a solution of 0.2 M Cu(I) as well as 0.04 M Cu(II) complexes, 0.1 M LiTFSI (lithium bis(trifluoromethylsulfonyl)imide) and 0.6 M tributyl phosphate (TBP) in acetonitrile. Supplementary Table 1 gives an overview of the photocurrent density–voltage characteristics of the DSCs co-sensitization series between D35 and XY1. We calculated the PCE values using equation (1), where J_{sc} is the short-circuit photocurrent density, V_{oc} the open-circuit voltage, FF the fill factor and I_o the intensity of incident light:

$$\mathrm{PCE} = J_{sc} \times V_{oc} \times \frac{\mathrm{FF}}{I_o} \quad (1)$$

For standard full AM 1.5G sunlight, we obtained the best conversion efficiency of 11.3% at a D35:XY1 ratio of 4:1 in the staining solution. We measured a J_{sc} of 16.2 mA cm^{-2} and a FF of 68%. V_{oc} values over 1.0 V were reached for the whole series, with a maximum of 1.1 V for pure D35. At a lower solar light intensity of 12 mW cm^{-2}, the

© 2017 Macmillan Publishers Limited, part of Springer Nature. All rights reserved.

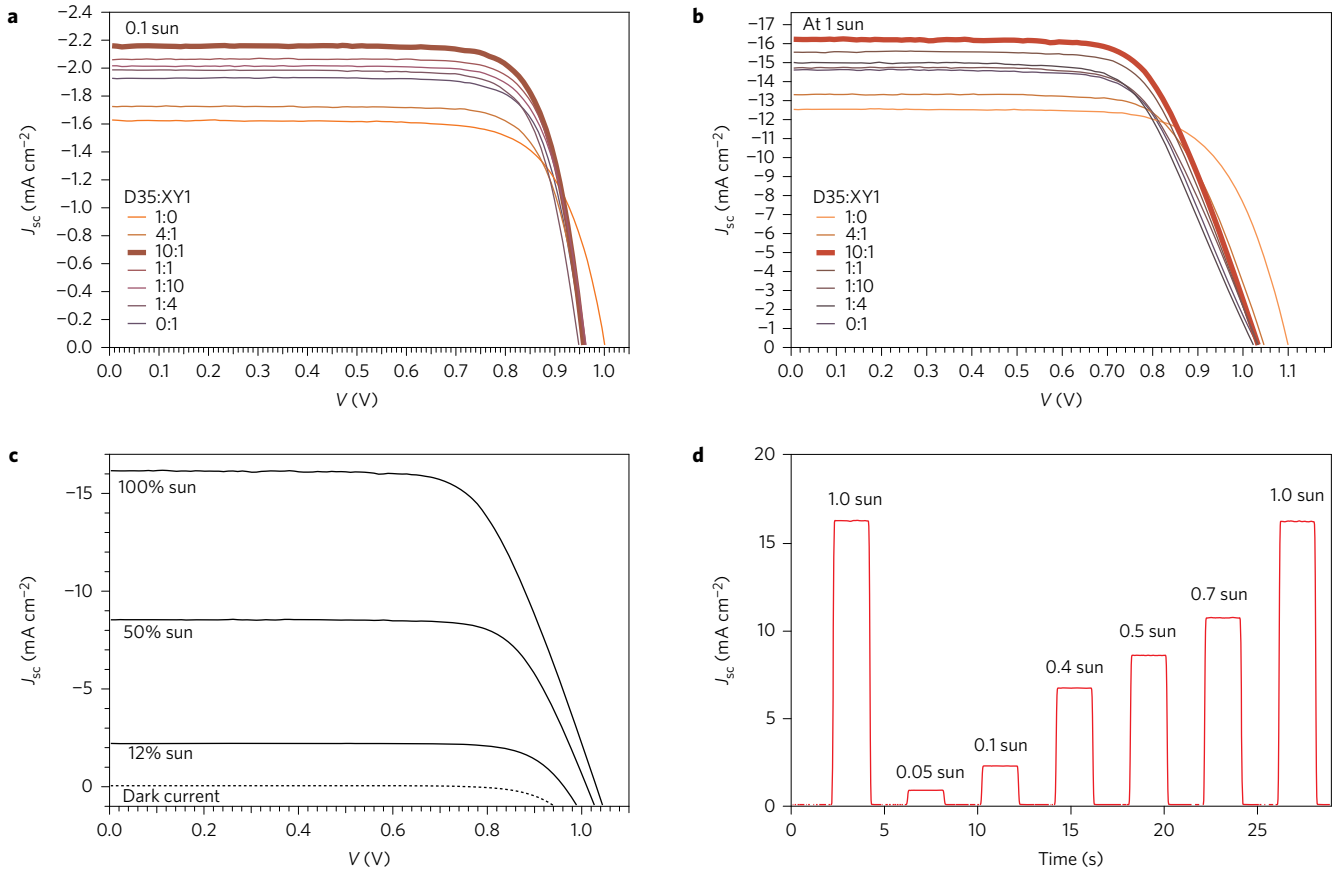

Figure 2 | Photovoltaic characteristics of D35/XY1 co-sensitized systems with Cu(tmby)$_2$ as the redox mediator. a,**b**, Measured *J*–*V* curves at 12 mW cm^{-2} (10% sun) (**a**) and 100 mW cm^{-2} (100% sun) (**b**) for various ratios of D35 and XY1. **c**, *J*–*V* curves of the champion solar cell at the ratio of 4:1 (D35:XY1) at 100, 50 and 12% sun (solid lines) and the corresponding dark currents (dashed line). **d**, Dependence of the photocurrent dynamics on the solar light intensity for the champion solar cell.

maximum PCE increased to 13% for the same staining solution; these are exceptionally high values for a solar cell system under these low light conditions (Fig. 2c). Here it is evident that both dyes complement each other in terms of photovoltaic performance—XY1 contributes to the large photocurrents because of its high molar extinction coefficient in the 500–650 nm wavelength region, and D35 supports the high V_{oc} values as it is endowed with groups that block sterically the access of the Cu(II)(tmby)$_2$ complex to the TiO_2 surface. This reduces the ability of the Cu(II) complex to recapture the photoinjected electrons from the TiO_2 conduction band. Figure 2d shows the photocurrent dynamics as a function at various light intensities for the best-performing DSC. The J_{sc} depends linearly on the light intensity and hence it is not limited by mass transport up to full sun illumination.

The incident photon to electron conversion efficiency (IPCE) spectra for the DSC at the various co-sensitization ratios, recorded at a 10% light-emitting diode bias light intensity, are shown in Fig. 3. For the best-performing co-sensitized system (4:1, D35:XY1), the IPCE reaches its highest values within the series of 91% at 540 nm. Considering the optical loss of the FTO substrate, the internal quantum efficiency ranges between 90% and practically 100% (380–600 nm). For comparison, DSCs that incorporate the single dye D35 show a lower IPCE of 80% at 540 nm and a narrower spectral response of the photocurrent, which is limited to the 380–550 nm wavelength domain. DSCs with only the XY1 sensitizer show a larger spectral coverage up to 640 nm, but a slightly lower IPCE of 88% at 540 nm.

The charge-extraction measurements as a function of V_{oc}, presented in Supplementary Fig. 1a, show a downshift of 70 mV of the conduction band edge for the best-performing co-sensitization ratio of the D35:XY1 dye (4:1). More charge is extracted at a lower V_{oc} especially in comparison with a DSC with only one of the two sensitizers. This is probably related to the optimal dye coverage between the two sensitizers on the TiO_2 layer. We employed the copper(II/I) complex-based electrolyte to measure electron lifetimes as a function of V_{oc} of the complete DSCs for the co-sensitized series. These are displayed in Supplementary Fig. 1b as a semilogarithmic plot of electron lifetime as a function of V_{oc}. The electron lifetimes of DSCs made at higher ratios of the D35 dye are longer than those obtained from the XY1-rich staining solutions. Given that the same electrolyte composition and redox mediators were used for all the studied solar cells, this indicates a higher rate of recombination for the XY1 dye. The curved shape of the slopes can be attributed to electron recombination from the FTO substrate (with a thin TiO_2 blocking layer) to the redox mediator. It is probable that the blocking layer contains pinholes, which become more apparent at lower light intensities[35].

Transient absorption and steady-state absorption spectroscopy. To gain better insight into the electron-transfer dynamics of the D35/XY1 co-sensitized mesoscopic TiO_2 films, time-resolved nanosecond transient and steady-state absorbance measurements were performed. In total, we examined seven dye-sensitized TiO_2 electrodes with different D35/XY1 loading ratios of 100% D35, 9% XY1, 20% XY1, 50% XY1, 80% XY1, 90% XY1 and 100% XY1. The relative surface coverage by the two sensitizers will differ from their concentration ratios in the staining solution. This

© 2017 Macmillan Publishers Limited, part of Springer Nature. All rights reserved.

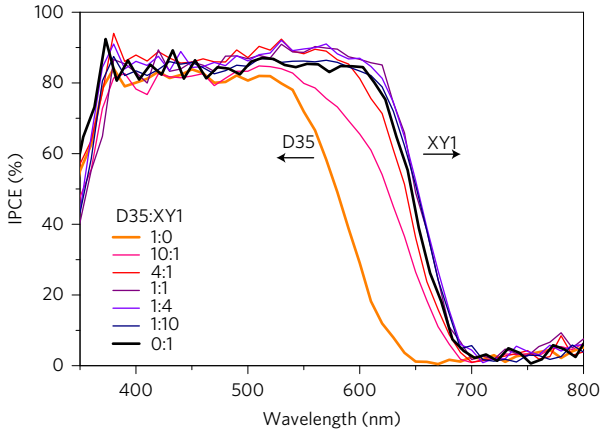

Figure 3 | IPCE spectra of DSCs co-sensitized at various dye ratios.

is confirmed by the absorption spectra of the sensitized TiO_2 (Fig. 4b). Photoinduced absorption spectroscopy (PIA) was performed to resolve the oxidized dyes spectra on TiO_2 along with bleaching of their ground states. We use this measurement to extract two wavelengths to monitor preferentially one oxidized dye or the other. Figure 4a shows that at 780 nm we mainly observe oxidized XY1 (oxidized D35 at its minimum absorbance and oxidized XY1 close to its maximum absorbance), whereas the 1,200 nm probing targets oxidized D35 (oxidized XY1 at its minimum absorbance and oxidized D35 close to its maximum absorbance). In between, a smooth transition is observed, which indicates that we effectively load the films with different concentration ratios. No significant lateral hole transfer takes place between both dyes as none of the two oxidized species is preferentially observed. From the PIA spectra, transient absorption spectroscopy (TAS) was performed at both wavelengths (780 and 1,200 nm) in the micro- to millisecond timescale to follow the transient decay of the dyes' oxidized species, and therefore recombination of the oxidized dyes with TiO_2 electrons or regeneration by the copper-based electrolyte. The time evolution of the transient absorption at 780 nm, which reflects the lifetime of oxidized XY1, does not appear to depend on the dye-concentration ratio. In an inert electrolyte, we observe similar lifetimes for the oxidized state of both dyes, that is, 2.10 and 1.85 ms for D35 and XY1, respectively (Fig. 4c). On the addition of the redox electrolyte that contains $Cu(tmby)_2$, both sensitizers are regenerated efficiently. From monitoring the transient absorption at 1,200 nm, we infer that the regeneration of D35 occurs with time constants that range from 2 to 10.8 µs and without any identifiable trend, whereas at 780 nm we observe the regeneration of XY1 oxidized molecules with time constants that range from 1.1 to 5.2 µs (Fig. 4d). Overall dye-regeneration yields are only marginally affected by these variations and are all above 99.5%, using pseudo-first-order rate constants for regeneration and first-order rate constants for recombination reactions.

DSCs performance under indoor-light conditions. Indoor-light conditions are very different compared with the solar irradiance outdoors, because the light intensity is orders of magnitude lower and the spectra of the indoor-light sources differs greatly from that of solar emission. Standard indoor illumination has an intensity between 200 and 2,000 lux. Illuminance is analogous to

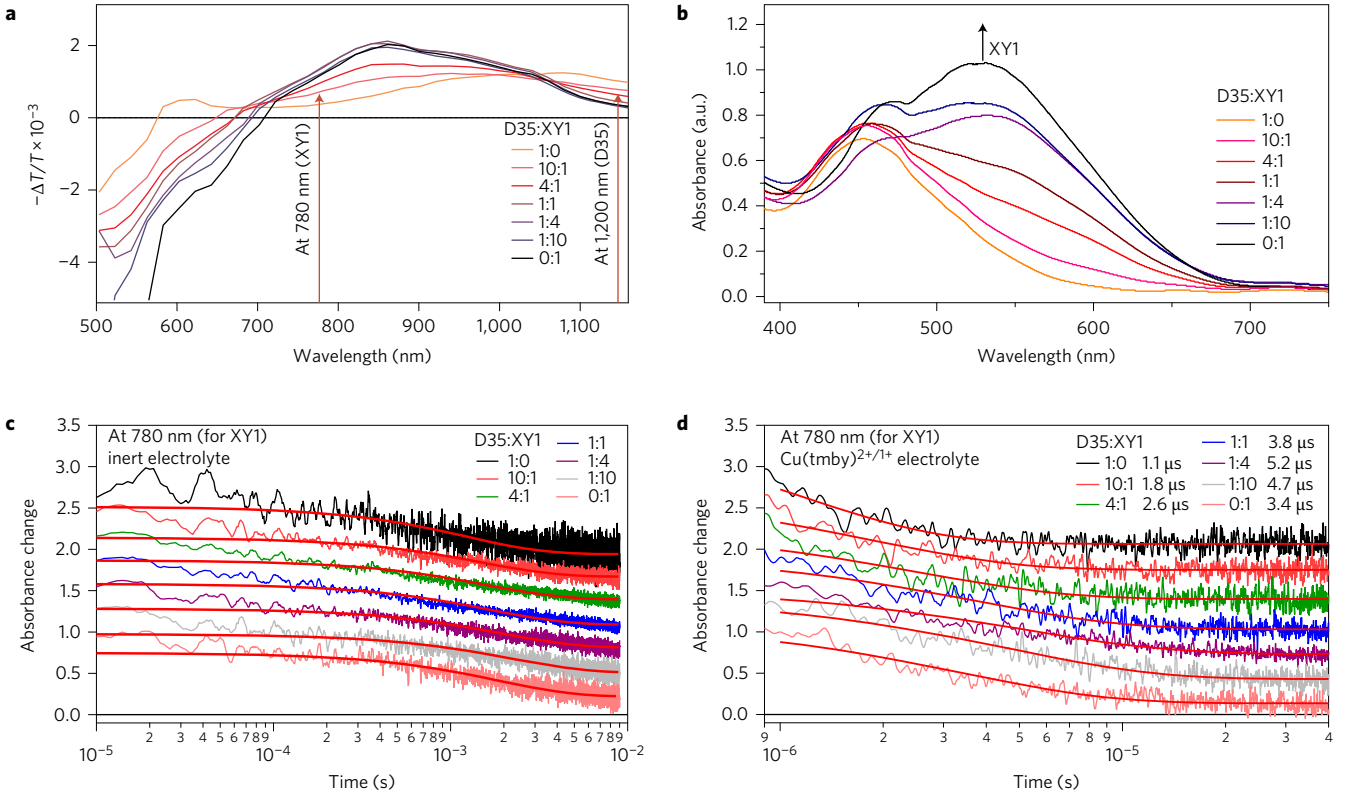

Figure 4 | Absorption spectroscopy and time-resolved laser spectroscopy of interfacial electron transfer that involve the D35 and XY1 sensitizers. **a**, Photoinduced absorption (PIA) spectra of dye-sensitized TiO_2 electrodes with different dye solution ratios of D35 and XY1 organic dyes. **b**, UV–vis absorption spectra of the corresponding sensitized TiO_2 substrates. **c**,**d**, Transient absorption decays of the sensitized TiO_2 films after 532 nm excitation with an inert (**c**) and $Cu(tmby)^{2+/1+}$-based (**d**) electrolyte. The red lines in both transient absorption decays represent the fits of the signal at the 4:1 D35:XY1 dye ratio. The curves of the transient absorption decays have an offset of 0.3 for better visualization.

© 2017 Macmillan Publishers Limited, part of Springer Nature. All rights reserved.

Table 1 | Photovoltaic metrics for DSCs and GaAs solar cells for indoor-light sources at 200 lux and 1,000 lux.

Solar cell	Light source	Light intensity (lux)	J_{sc} (μA cm^{-2})	V_{oc} (mV)	FF (%)	P_{in} (μW cm^{-2})	P_{out} (μW cm^{-2})	PCE (%)
DSC*	Osram Warm White 930	200	27.2	732.0	0.79	61.3	15.6	25.5
DSC†		200	24.8	700.0	0.79	61.3	13.7	22.3
DSC*		1,000	138.0	797.0	0.80	306.6	88.5	28.9
DSC†		1,000	137.2	766.0	0.80	306.6	84.1	27.4
Flexi-GaAs (Alta)	Osram Warm White 827	200	20.1	870.0	0.75	70.6	13.1	18.6
Flexi-GaAs (Alta)		1,000	99.0	940.0	0.80	354.0	74.5	21.0

*Acetonitrile-based electrolyte. †Propionitrile-based electrolyte. The PCEs for the solar cells are determined from equation (2). Flexi-GaAs solar cells are from Alta Devices measured at GCell with a configuration of six cells of area 8.33 cm^2 in parallel and in series connected to a mini-module of size 50 cm^2.

irradiance (watts per square metre) commonly used for outdoor devices, but relates the intensity to how it is perceived by humans instead of power[36]. As a comparison between the two units, full solar irradiation, that is, 100 mW cm^{-2} AM 1.5G, corresponds to about 100,000–110,000 lux. Therefore, indoor light at 1,000 lux corresponds to ~1% of the standard AM 1.5G solar irradiation[37–39].

As relatively few reports exist that focus on the use of DSCs for indoor-light harvesting, no standard indoor-light source has been established so far. We chose a typical light tube, Osram Warm White 930 (representative spectra of the light source are given in Supplementary Figs 5 and 6), to test the DSCs under realistic indoor conditions. We measured the light intensity that strikes the DSC by using of a lux meter (TES 1334).

The DSCs fabricated for the study of indoor-light conditions have a larger area of 2.8 cm^2 compared with the normally used laboratory test DSCs (0.22 cm^2). The purpose behind this is to have a smaller discrepancy between 'real-life application' and laboratory-produced solar cells, which tend to have a better efficiency attributed to their smaller size. Further, the DSCs with a less volatile electrolyte solvent, propionitrile, were compared with the DSCs using the standard electrolyte composition that contained acetonitrile[23]. Otherwise, the same composition for the Cu(II/I)(tmby)$_2$ was applied. The mesoscopic TiO_2 films were sensitized with D35 and XY1 dyes in a staining solution that contained 0.08 mM D35 and 0.02 mM XY1 (ratio of 4:1).

The PV metrics and power output (P_{out}) of the DSCs and GaAs solar cells (flexi-GaAs (Alta Devices)) were compared under similar indoor-light conditions (Table 1). The efficiencies of the solar cells at indoor conditions were calculated with equation (2), where P_{out} (W cm^{-2}) is the output power of the solar cell and P_{in} (W cm^{-2}) is the incident power of the light source, measured by a calibrated Si-diode or the lux meter:

$$\eta = \frac{P_{out}}{P_{in}} \quad (2)$$

Given that the spectral region in which the DSCs absorb light is limited to the visible part of the solar spectrum, it is expected that their efficiency in the visible region (400–700 nm) is twice the full-spectrum value[20]. Taking into consideration that the indoor-light sources emit mostly visible light, a DSC with an 11.3% PCE under full solar illumination is expected to have an efficiency over 20% in its particular spectrum of operation indoors. When an indoor-light source was used, the DSCs outperformed the GaAs solar cells under similar conditions. The illumination intensity of the indoor-light sources was varied between 200 and 1,000 lux and, in both cases, the power output of the DSCs was higher. At 200 lux, the best-performing DSC yields a power output of 15.6 μW cm^{-2} (the average of 19 samples was 13.5 μW cm^{-2}), which is substantially higher than the 13.1 μW cm^{-2} obtained for GaAs. At 1,000 lux, the best DSC gives 88.5 μW cm^{-2} (the average of seven samples was 80.0 μW cm^{-2}), again clearly above the 74.5 μW cm^{-2} produced by GaAs (Fig. 5 and Table 1). This translates into a PCE of 28.9% for the DSC that operates at 1,000 lux. Low-power electronic devices, such as wireless sensor nodes or low-power microcontroller units, typically consume about 100 μW in sleeping mode[40–42]. Roundy *et al.* illustrate that at this average power consumption, a 1 cm^3 primary battery (0.8 W h cm^{-3}) lasts for about 11 months, before the node goes into an idle state[43]. A 2 cm^2 DSC would therefore be able to render the low-power device fully autonomous[43].

We advance the following rationale to explain the outstanding ambient light performance of dye-sensitized solar cells that employ a combination of the two sensitizers with the Cu(II/I) redox-elect electrolyte:

(1) The co-sensitization of mesoscopic titania scaffolds by the two sensitizers with complementary absorption spectra extends the light-harvesting ability of the device over a wider spectral domain, which increases its short-circuit photocurrent. In the present case, the D35 absorbs mainly blue and green light, whereas the XY1 covers the yellow and red spectral region.
(2) The sensitizers are judiciously engineered on the molecular scale such that their electron-acceptor moiety, the cyanoacrylate group, is attached by coordinative bonding to the titanium ions surface of the TiO_2, whereas their arylamine donor group is positioned away from the interface at the opposite end of the dye molecule. In the chemical design of the sensitizer structure their lowest unoccupied molecular orbital is adjusted to match the energy of the conduction band edge of TiO_2 formed by the Ti (3*d*) orbitals. In this way, the energy loss associated with the interfacial electron-injection process is minimized. Optical excitation promotes electrons from the donor to

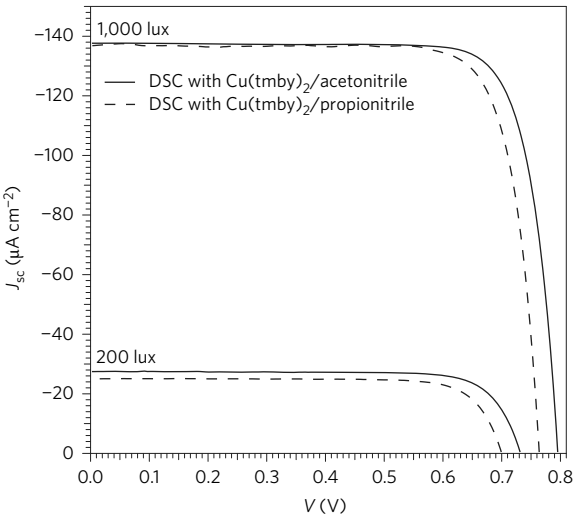

Figure 5 | Photovoltaic characteristics of co-sensitized DSCs measured under indoor-light conditions. *J*–*V* curves at 200 lux and 1,000 lux of DSCs for the co-sensitized dyes D35:XY1 (4:1) with the Cu(tmby)$_2$ acetonitrile-based electrolyte (solid line) and the Cu(tmby)$_2$ propionitrile-based electrolyte (dashed line).

© 2017 Macmillan Publishers Limited, part of Springer Nature. All rights reserved.

the acceptor moiety of the sensitizer, which enhances their electronic coupling with the Ti ($3d$) orbitals at the TiO_2 surface, such that the interfacial electron transfer from the excited sensitizer into the TiO_2 can proceed very rapidly, that is, in the femtoseconds- to picoseconds time range. By contrast, the long distance between the electron in the TiO_2 and the hole that is localized on the terminal arylamine group of the sensitizer weakens their electronic interactions, which results in time constants for the recombination reaction in the milliseconds to seconds domain.

(3) The two sensitizers undergo synergistic interactions in the adsorbed state. Thus, the second dye may suppress unfavourable interactions of the first dye with the TiO_2 surface or with itself (dye aggregation). This effect enhances the spectral response of the photocurrent of the first dye[44].

(4) The two sensitizers together form a more tightly packed monolayer at the surface than the individual dyes can. This blocks the approach of the Cu(II) complex to the surface, which retards the unwanted back-electron transfer reaction and so increases the V_{oc} of the device.

(5) The close matching of the redox potentials of the sensitizers with that of the Cu(II/I) complexes used as a redox shuttle means the V_{oc} values achieved are much higher than those achieved with the conventional iodide/triiodide redox system.

Conclusions

We introduce a new DSC design that combines two judiciously selected sensitizers and so enables incident light to be harvested over the whole visible range. We use Cu(II/I)$(tmby)_2$ as a redox relay, which is capable of successfully regenerating both dyes at only a 0.1–0.2 eV driving force. In standard AM 1.5G sunlight, the PCE reaches 11.3%, a new record for a system based on a copper electrolyte. Strikingly, under 1,000 lux the indoor illumination PCE of this new DSC design is 28.9%, which results in a power output of 88.5 μW cm^{-2}. It is sufficient to ascertain the autonomous operation of a range of electronic devices in an indoor environment with a reasonable solar cell size. Therefore, our study suggests that DSCs are ideally suited for ambient light applications. We expect our findings to have a major practical impact, because harvesting the ambient light energy to power electronic devices or to extend their battery lifetime will open a wide field of applications in a wide range of systems that require electric power for their autonomous operation.

Methods

Methods and any associated references are available in the online version of the paper.

Received 8 December 2016; accepted 27 March 2017;
published online 1 May 2017; corrected online 8 May 2017

References

1. Collins, S. & Bell, G. Phenotypic consequences of 1,000 generations of selection at elevated CO_2 in a green alga. *Nature* **431,** 566–569 (2004).
2. Rogelj, J. *et al.* Paris Agreement: climate proposals need a boost to keep warming well below 2 °C. *Nature* **534,** 631–639 (2016).
3. Ashina, S., Fujino, J., Masui, T., Ehara, T. & Hibino, G. A roadmap towards a low-carbon society in Japan using backcasting methodology: feasible pathways for achieving an 80% reduction in CO_2 emissions by 2050. *Energy Policy* **41,** 584–598 (2012).
4. Wackernagel, M. & Rees, W. *Our Ecological Footprint: Reducing Human Impact on the Earth* (New Society, 1998).
5. Green, M. A. Third generation photovoltaics: solar cells for 2020 and beyond. *Physica E* **14,** 65–70 (2002).
6. Repins, I. *et al.* 19.9%-efficient ZnO/CdS/$CuInGaSe_2$ solar cell with 81.2% fill factor. *Prog. Photovolt. Res. Appl.* **16,** 235–239 (2008).
7. Chopra, K. L., Paulson, P. D. & Dutta, V. Thin-film solar cells: an overview. *Prog. Photovolt. Res. Appl.* **12,** 69–92 (2004).
8. Saliba, M. *et al.* Incorporation of rubidium cations into perovskite solar cells improves photovoltaic performance. *Science* **354,** 206–209, (2016).
9. Li, X. *et al.* A vacuum flash-assisted solution process for high-efficiency large-area perovskite solar cells. *Science* **353,** 58–62 (2016).
10. Green, M. A., Ho-Baillie, A. & Snaith, H. J. The emergence of perovskite solar cells. *Nat. Photon.* **8,** 506–514 (2014).
11. Mathew, S. *et al.* Dye-sensitized solar cells with 13% efficiency achieved through the molecular engineering of porphyrin sensitizers. *Nat. Chem.* **6,** 242–247 (2014).
12. O'Regan, B. & Gratzel, M. A low-cost, high-efficiency solar cell based on dye-sensitized colloidal TiO_2 films. *Nature* **353,** 737–740 (1991).
13. Fraas, L. M. & Partain, L. D. *Solar Cells and Their Applications* (Wiley, 2010).
14. Kalyanasundaram, K. *Dye-Sensitized Solar Cells* (EFPL, 2010).
15. Sakamoto, R. *et al.* Electron transport dynamics in redox-molecule-terminated branched oligomer wires on Au(111). *J. Am. Chem. Soc.* **137,** 734–741 (2015).
16. Mathews, I., King, P. J., Stafford, F. & Frizzell, R. Performance of III–IV solar cells as indoor light energy harvesters. *IEEE J. Photovolt.* **6,** 230–235 (2016).
17. Yang, P. C., Chan, I. M., Lin, C. H. & Chang, Y. L. Thin film solar cells for indoor use. In *37th IEEE Photovoltaic Specialists Conf.*, 696–698 (IEEE, 2011).
18. Hagfeldt, A., Boschloo, G., Sun, L., Kloo, L. & Pettersson, H. Dye-sensitized solar cells. *Chem. Rev.* **110,** 6595–6663 (2010).
19. Barber, G. D. *et al.* Utilization of direct and diffuse sunlight in a dye-sensitized solar cell—silicon photovoltaic hybrid concentrator system. *J. Phys. Chem. Lett.* **2,** 581–585 (2011).
20. Lechêne, B. P. *et al.* Organic solar cells and fully printed super-capacitors optimized for indoor light energy harvesting. *Nano Energy* **26,** 631–640 (2016).
21. Lan, J.-L., Wei, T.-C., Feng, S.-P., Wan, C.-C. & Cao, G. Effects of iodine content in the electrolyte on the charge transfer and power conversion efficiency of dye-sensitized solar cells under low light intensities. *J. Phys. Chem. C* **116,** 25727–25733 (2012).
22. Kroon, J. M. *et al.* Nanocrystalline dye-sensitized solar cells having maximum performance. *Prog. Photovolt. Res. Appl.* **15,** 1–18 (2007).
23. Kontos, A. G. *et al.* Long-term thermal stability of liquid dye solar cells. *J. Phys. Chem. C* **117,** 8636–8646 (2013).
24. Hattori, S., Wada, Y., Yanagida, S. & Fukuzumi, S. Blue copper model complexes with distorted tetragonal geometry acting as effective electron-transfer mediators in dye-sensitized solar cells. *J. Am. Chem. Soc.* **127,** 9648–9654 (2005).
25. Bai, Y. *et al.* High-efficiency organic dye-sensitized mesoscopic solar cells with a copper redox shuttle. *Chem. Commun.* **47,** 4376–4378 (2011).
26. Freitag, M. *et al.* High-efficiency dye-sensitized solar cells with molecular copper phenanthroline as solid hole conductor. *Energy Environ. Sci.* **8,** 2634–2637 (2015).
27. Saygili, Y. *et al.* Copper bipyridyl redox mediators for dye-sensitized solar cells with high photovoltage. *J. Am. Chem. Soc.* **138,** 15087–15096 (2016).
28. Freitag, M. *et al.* Copper phenanthroline as a fast and high-performance redox mediator for dye-sensitized solar cells. *J. Phys. Chem. C* **120,** 9595–9603 (2016).
29. Mathews, I., Kelly, G., King, P. J. & Frizzell, R. GaAs solar cells for indoor light harvesting. In *40th Photovoltaic Specialist Conf.*, 510–513 (IEEE, 2014).
30. Feldt, S. M. *et al.* Design of organic dyes and cobalt polypyridine redox mediators for high-efficiency dye-sensitized solar cells. *J. Am. Chem. Soc.* **132,** 16714–16724 (2010).
31. Hagberg, D. P. *et al.* Symmetric and unsymmetric donor functionalization. Comparing structural and spectral benefits of chromophores for dye-sensitized solar cells. *J. Mater. Chem.* **19,** 7232–7238 (2009).
32. Zhang, X. *et al.* Molecular engineering of potent sensitizers for very efficient light harvesting in thin-film solid-state dye-sensitized solar cells. *J. Am. Chem. Soc.* **138,** 10742–10745 (2016).
33. Honda, M., Yanagida, M. & Han, L. Effect of co-adsorption dye on the electrode interface (Ru complex/TiO_2) of dye-sensitized solar cells. *AIP Adv.* **3,** 72113 (2013).
34. Ellis, H. *et al.* PEDOT counter electrodes for dye-sensitized solar cells prepared by aqueous micellar electrodeposition. *Electrochim. Acta* **107,** 45–51 (2013).
35. Rühle, S. *et al.* Molecular adjustment of the electronic properties of nanoporous electrodes in dye-sensitized solar cells. *J. Phys. Chem. B* **109,** 18907–18913 (2005).
36. De Rossi, F., Pontecorvo, T. & Brown, T. M. Characterization of photovoltaic devices for indoor light harvesting and customization of flexible dye solar cells to deliver superior efficiency under artificial lighting. *Appl. Energy* **156,** 413–422 (2015).
37. Reich, N. H., van Sark, W. G. J. H. M. & Turkenburg, W. C. Charge yield potential of indoor-operated solar cells incorporated into product integrated photovoltaic (PIPV). *Renew. Energy* **36,** 642–647 (2011).
38. Tian, H. & Sun, L. Iodine-free redox couples for dye-sensitized solar cells. *J. Mater. Chem.* **21,** 10592–10601 (2011).
39. Randall, J. F. & Jacot, J. Is AM1.5 applicable in practice? Modelling eight photovoltaic materials with respect to light intensity and two spectra. *Renew. Energy* **28,** 1851–1864 (2003).
40. Tan, Y. K. & Panda, S. K. Energy harvesting from hybrid indoor ambient light and thermal energy sources for enhanced performance of wireless sensor nodes. *IEEE Trans. Ind. Electron.* **58,** 4424–4435 (2011).

© 2017 Macmillan Publishers Limited, part of Springer Nature. All rights reserved.

41. Borgeson, J., Schauer, S. & Diewald, H. *Benchmarking MCU Power Consumption for Ultra-Low-Power Applications* (Texas Instruments, 2012).
42. Dolgov, A., Zane, R. & Popovic, Z. Power management system for online low power RF energy harvesting optimization. *IEEE Trans Circuits Systems I* **57,** 1802–1811 (2010).
43. Roundy, S. *et al.* Improving power output for vibration-based energy scavengers. *IEEE Pervasive Comput.* **4,** 28–36 (2005).
44. Ogura, R. Y. *et al.* High-performance dye-sensitized solar cell with a multiple dye system. *Appl. Phys. Lett.* **94,** 73308 (2009).

Acknowledgements

We acknowledge the Swiss National Science Foundation for financial support with the project entitled 'Fundamental studies of mesoscopic devices for solar energy conversion', project no. 200021_157135/1, and the NCCR MUST research instrument. J.H. and X.Y. thank NSFC/China (21421004 and 91233207) and the Programme of Introducing Talents of Discipline to Universities (B16017). We appreciate the technical support of R. Humphry-Baker, P. Comte and J.-D. Decoppet. We are also very grateful to G24power for the comparative measurements of the GaAs Alta solar cells under indoor-light conditions.

Author contributions

A.H. supervised the study. M.F. conceived the work and designed the experiments. M.F. and M.G. wrote the manuscript with feedback from the co-authors. M.F., P.L. and Y.S. fabricated and characterized the solar cells. M.F. assembled the devices, and analysed and synthesized the copper complexes. Y.S. prepared the PEDOT counter electrodes. X.Z. and J.H. were responsible for the XY1 dye synthesis and characterization. J.T. and J.-E.M. performed and analysed the PIA and transient spectroscopy measurements. F.G. contributed to the electrolyte and device characterization. S.M.Z. and M.G. coordinated the work.

Additional information

Supplementary information is available in the online version of the paper. Reprints and permissions information is available online at www.nature.com/reprints. Publisher's note: Springer Nature remains neutral with regard to jurisdictional claims in published maps and institutional affiliations. Correspondence and requests for materials should be addressed to M.G. and A.H.

Competing financial interests

The authors declare no competing financial interests.

© 2017 Macmillan Publishers Limited, part of Springer Nature. All rights reserved.

Methods

Fabrication of solar cells. Generally, the solar cells were fabricated as previously described[11,27]. The FTO substrates (NSG-10, Nippon Sheet Glass) were first cleaned with a detergent solution (Deconex) in ultrasonic bath (45 min) and rinsed with water and ethanol. This initial step was followed by a 15 min ultraviolet/O_3 treatment (Model no. 256–220, Jelight). Then the substrates were immersed into a 53 mM $TiCl_4$ solution and kept at 70 °C in an oven for 30 min to allow the formation of a thin and compact TiO_2 underlayer. After 30 min the substrates were rinsed with water and ethanol. The $TiCl_4$ treatment was followed by a 2 h annealing process at 250 °C. Two layers of mesoporous TiO_2 layers were prepared on top of the underlayer; the first layer was screen printed using a paste that consisted of 30 nm diameter TiO_2 particles (Dyesol) and the second one with 400 nm particles (light-scattering layer), which results in a thickness of 8 μm of TiO_2 (4 μm 30NRD + 4 μm scattering layer)[45]. TiO_2 films were immersed in dye solutions in acetonitrile/*tert*-butanol (v/v, 1/1) for 16 h to graft the dye molecules onto the TiO_2 surface. The sensitizing solutions contained the organic dyes in the following millimolar concentrations: 0.1 mM D35, 0.1 mM D35 and 0.01 mM XY1 (D35:XY1, 10:1), 0.08 mM D35 and 0.02 mM XY1 (4:1), 0.05 mM D35 and 0.05 mM XY1 (1:1), 0.02 mM D35 and 0.08 mM XY1 (1:4), 0.01 mM D35 and 0.1 mM XY1 (1:10) and 0.1 mM XY1.

We used FTO glass covered with electrochemically deposited PEDOT films as counter electrodes[34]. The dye-coated TiO_2 film and the counter electrode were assembled by using a thermoplastic frame (Surlyn, DuPont) heated at 120 °C. Electrolyte was injected into the space between the electrodes through a pre-drilled hole on the counter electrode under vacuum. The electrolyte consisted of a solution of 0.2 M Cu(I) and 0.04 M Cu(II) complexes and 0.1 M LiTFSI as well as 0.6 M TBP in acetonitrile. The hole was sealed by using a polymer hot melt (Surlyn). The DSCs prepared with TiO_2 of area 2.8 cm^2 were assembled using ultraviolet glue (Three Bond: 3035B).

Characterization of solar cells. The characterizations of the current–voltage (J–V) and IPCE of solar cells are described in the literature[11]. The device J–V characteristics were obtained by using a 450 W xenon light source (Oriel). A Keithley model 2400 digital source meter was used to apply an external potential bias to the devices and measure the resulting current. IPCE data were acquired using a modulated light intensity with a frequency of 1 Hz. The light, from a 300 W xenon light source (ILC Technology), was focused through a monochromator (JobinYvon) and directed to the device under test. A white-light bias was used to have similar light-intensity conditions as those in normal operation. The solar cells (without antireflection films) were masked to attain an illuminated active area of 0.158 cm^2.

Large-area solar cells (2.8 cm^2) were covered with a mask of the same aperture. The low-light measurements were performed using an Osram Warm White 930 and Philips-Warm White (PL Electronic-C) discharge tubes for DSCs and Osram Warm White 827 lamp for GaAs solar cells. A TES-1334 luxmeter was used to measure the light intensity. Flexi-GaAs solar cells are from Alta Devices measured at GCell with the configuration: six cells in parallel and series (of 8.33 cm^2) as the module (50 cm^2). The luxmeter TES-1334 was used to measure the light intensity at the DSC. In summary, 63 small-area (three solar cells per condition for seven conditions, where each was repeated three times) and 15 large-area solar cells were tested. The PCE distribution was within ±0.5%. Care was taken to scan the J–V curve sufficiently slowly so that any hysteresis effect on the maximum power point remained below 2%. Hysteresis was checked by scanning the J–V curve in forward and backward directions and comparing the PV metrics obtained for the two scanning directions.

Ultraviolet–visible (UV–vis) spectroscopy. UV–vis absorption data were collected using a Perkin-Elmer Lambda 950 spectrophotometer.

Extracted charge and electron-lifetime measurements. Electron-lifetime measurements were performed using the DN-AE01 Dyenamo toolbox with a white light-emitting diode (Luxeon Star 1W) as the light source[46]. Voltage traces were recorded with a 16-bit resolution digital acquisition board (National Instruments) and lifetimes were determined by monitoring photovoltage transients at different light intensities on applying a small square-wave modulation to the base light intensity. The photovoltage response was fitted using first-order kinetics to obtain the time constants.

TAS and PIA. The photoinduced kinetics were measured with an Ekspla NT-342 Q-switched neodymium:yttrium–aluminium–garnet laser using a 532 nm excitation wavelength. The pulse width was 4–5 ns (full-width at half-maximum) and the repetition rate was 20 Hz. The probe light source was a halogen lamp and probe wavelengths at 780 and 1,200 nm were chosen using a monochromator (Omni-λ 150, Oriel). The film was positioned at an approximately 45° angle with respect to the incoming laser pulse, for front illumination. The signal was detected using a photomultiplier tube (R9110, Hamamatsu) in the visible and an InGaAs diode (SM05PD5A, Thorlabs) in the near infrared, and then recorded using an oscilloscope (DPO 7014, Tektronix). The radiant output of the laser was attenuated to 50 μJ cm^{-2} using grey optical density filters. A low light-intensity value was deliberately chosen to ensure that, on average, less than one electron was injected per nanoparticle, and lifetimes were obtained fitting the data with a monoexponential function (Supplementary Information gives the details (Supplementary equation (1)). Satisfactory signal-to-noise ratios were typically obtained by averaging over 1,000 laser shots.

The PIA spectra of the various cells were recorded over a wavelength range of 500–1,160 nm after an (on/off) photomodulation using a 9 Hz square-wave that emanated from a blue laser (405 nm). White probe light from a halogen lamp (20 W) was used as an illumination source. The light was focused onto the sample, sent into a monochromator (Gemini, Horiba) and detected using a photodiode connected to a lock-in amplifier (SR830, Stanford Research Systems).

Data availability. The data that support the plots within this paper and other findings of this study are available from the corresponding author on reasonable request.

References

45. Bach, U. *et al.* Solid-state dye-sensitized mesoporous TiO_2 solar cells with high photon-to-electron conversion efficiencies. *Nature* **395,** 583–585 (1998).
46. Boschloo, G., Häggman, L. & Hagfeldt, A. Quantification of the effect of 4-*tert*-butylpyridine addition to I^-/I_3^- redox electrolytes in dye-sensitized nanostructured TiO_2 solar cells. *J. Phys. Chem. B* **110,** 13144–13150 (2006).

© 2017 Macmillan Publishers Limited, part of Springer Nature. All rights reserved.

nature photonics

SUPPLEMENTARY INFORMATION

DOI: 10.1038/NPHOTON.2017.60

In the format provided by the authors and unedited.

Dye-sensitized solar cells for efficient power generation under ambient lighting

Marina Freitag, Joël Teuscher, Yasemin Saygili, Xiaoyu Zhang, Fabrizio Giordano, Paul Liska, Jianli Hua, Shaik M. Zakeeruddin, Jacques-E. Moser, Michael Grätzel and Anders Hagfeldt

Materials.

Acetonitrile and propionitrile (Abcr), tert-butanol (Sigma-Aldrich), TiO_2 paste (30 NR-D, Dyesol), LiTFSI (TCI), TBP (TCI), tmby (hetcat) and D35 dye (Dyenamo) were purchased from commercial sources and used as received, unless stated otherwise. TiO_2 paste for scattering film was prepared as previously described.[48] The $[Cu^{I}(tmby)_2]TFSI$, and $[Cu^{II}(tmby)_2](TFSI)Cl$ and the dye XY1were synthesized as previously described.[28,35]

Photovoltaic characteristics characteristics of DSCs using co-sensitized photoanodes with D35 and XY1

Table S1 J-V characteristics of DSCs using co-sensitized photoanodes with D35 and XY1 dye at 12 and 100mWcm^{-2} simulated solar light intensity, letters in the first column refer to labels of sensitizing solutions, which contain: (a) 0.1mM D35, (b) 0.1mM D35 and 0.01mM XY1 (c) 0.08mM D35 and 0.02mM XY1, (d) 0.05 mM D35 and 0.05 mM XY1, (e) 0.02 mM D35 and 0.08 mM XY1, (f) 0.01mM D35 and 0.1 mM XY1(1:10), (g) 0.1 mM XY1.

#	Ratio of D35:XY1 (sensitizing solution)	Incident light intensity I_0 (mWcm^{-2})	J_{sc} (mA cm^{-2})	Voc (V)	FF (%)	n (%)
a	01:00	12	1,63	1,01	74	9,90
b	10:01		1,73	0,96	78	10,6
c	**04:01**		**2,17**	**0,96**	**78**	**13,2**
d	01:01		2,07	0,96	79	12,6
e	01:04		2,03	0,97	78	12,3
f	01:10		2,00	0,95	78	11,9
g	00:01		1,94	0,96	78	11,8
a	01:00	100	12,48	1,10	72	9,90
b	10:01		13,26	1,05	71	9,90
c	**04:01**		**16,19**	**1,03**	**68**	**11,3**
d	01:01		15,54	1,03	68	10,8
e	01:04		14,66	1,03	67	10,1
f	01:10		15,00	1,02	66	10,1
g	00:01		14,56	1,02	67	10,2

© 2017 Macmillan Publishers Limited, part of Springer Nature. All rights reserved.

Extracted charge at open circuit voltage (V_{oc}) and electron lifetime as function of V_{oc}

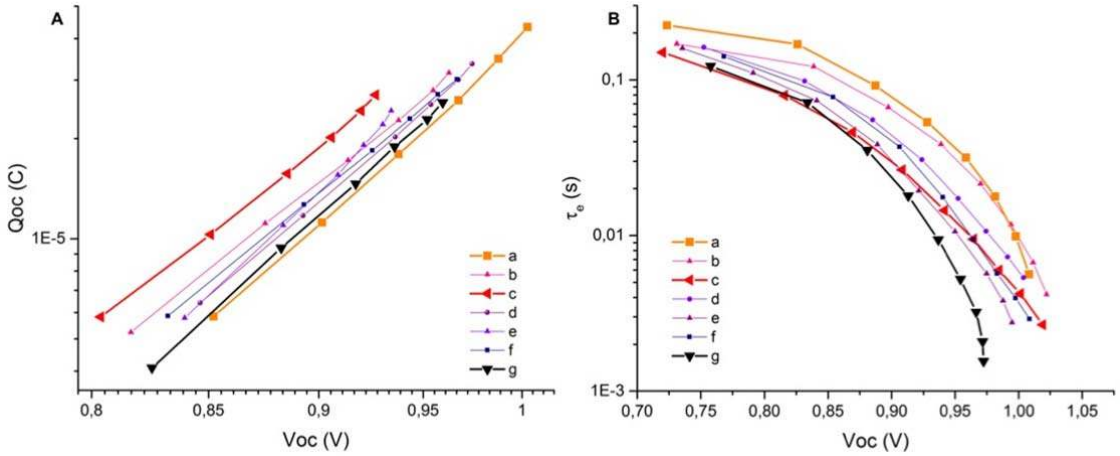

Figure S1. Extracted charge at open circuit voltage (V_{oc}) and electron lifetime as function of V_{oc}. Left panel: Extracted charge at open circuit voltage (V_{OC}) and right panel: electron lifetime as function of V_{oc} for DSCs employing pure (a) D35, (b) 10:1 D35:XY1, (c) 4:1 D35:XY1, (d) 1:1 D35:XY1, (e) 1:4 D35:XY1, (f) 1:10 D35:XY1, to (g) XY1

UV-Vis spectroscopy of the dyes (XY1 and D35) and the redox mediator ($Cu(tmby)_2^{1+/2+}$)

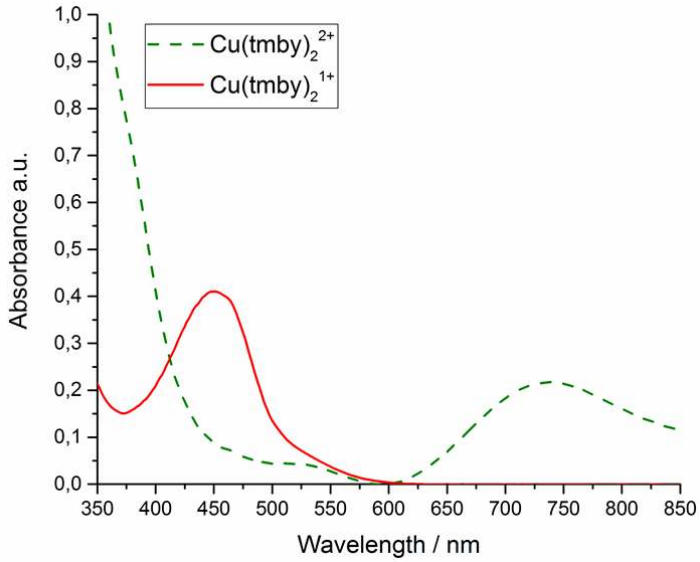

Figure S2. UV-Vis spectra of $Cu(tmby)_2TFSI_{1/2}$ in acetonitrile solution. Concentrations of the complexes were 0.5 mM of $Cu(tmby)_2^{1+}$ (red solid curve) and $Cu(tmby)_2^{2+}$ (green dashed curve).

© 2017 Macmillan Publishers Limited, part of Springer Nature. All rights reserved.

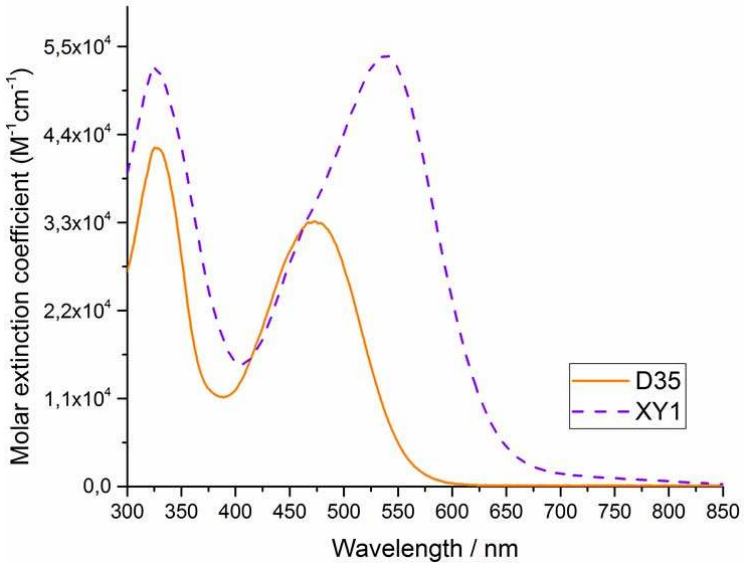

Figure S3. UV-Vis spectra of the dyes D35 (orange solid line) and XY1 (purple dashed line).

The transient absorption decays.

The lifetimes were obtained fitting the data with monoexponential function:

$$\Delta A(t) = A \cdot e^{\frac{-t}{\tau}} \qquad \text{Equation S1}$$

Power out distribution for DSCs and GaAs solar cells

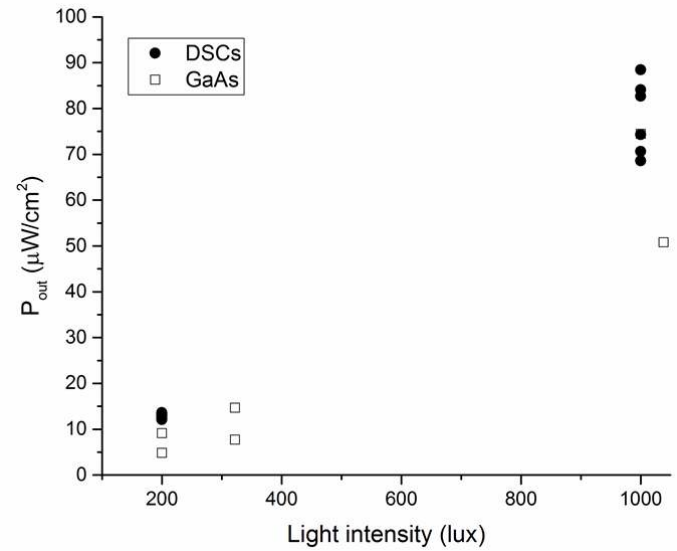

Figure S4. Output power under indoor light intensities (200-1000 lux). The solid black circle symbol indicates the values for DSCs under the Osram 930 lamp and square solid black lined symbols GaAs modules under Osram 827 lamp.

© 2017 Macmillan Publishers Limited, part of Springer Nature. All rights reserved.

GaAs solar cells

The flexi-GaAs-module is from Alta Devices measured at Gcell-company with the following configuration: 6 cells (of 8.33cm^2) as module (50cm^2) with parallel and series connections as 2 groups of 3 cells (in parallel) measured in series = 2 cells(2x25cm^2) in series.

Indoor light sources

The indoor light sources OSRAM Warm White 827 hat 1.77 W/m^2 was used at Gcell for GaAs and OSRAM Warm White 930 hat 1.566 W/m2 was used at EPFL for DSCs.

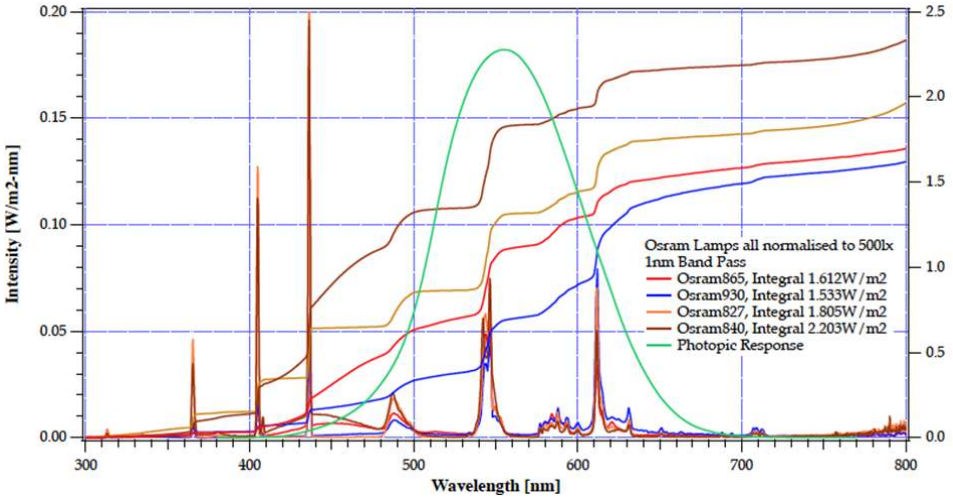

Figure S5. Normalized power spectra of various indoor light sources. For this study OSRAM Warm White 827 (orange, solid line) and OSRAM Warm White 930 (blue, solid line) were used.

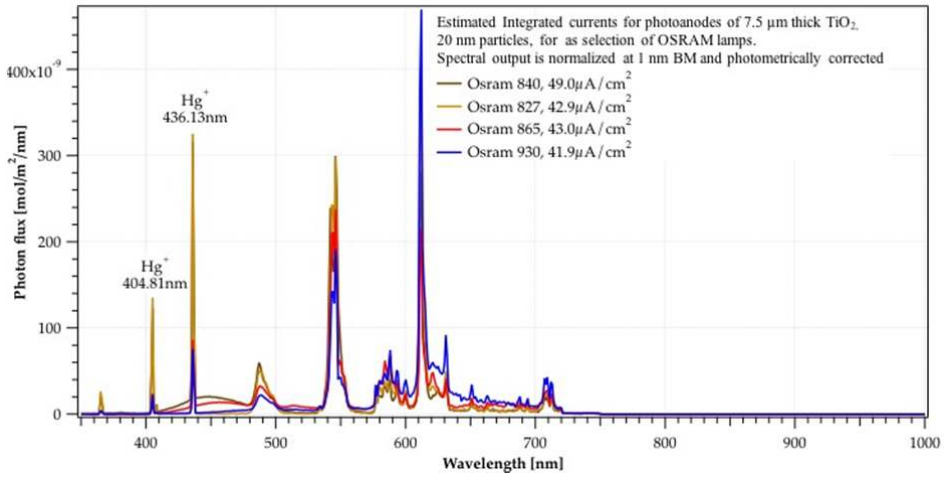

Figure S6. Normalized power spectra of various indoor light sources with estimated integrated currents of TiO_2 photoanodes. For this study OSRAM Warm White 827 (orange, solid line) and OSRAM Warm White 930 (blue, solid line) were used.

© 2017 Macmillan Publishers Limited, part of Springer Nature. All rights reserved.